High-angle wave instability and emergent shoreline shapes:
2. Wave climate analysis and comparisons to nature

Andrew D. Ashton[1,2] and A. Brad Murray[1]

[1] Recent research has revealed that the plan view evolution of a coast due to gradients in alongshore sediment transport is highly dependant upon the angles at which waves approach the shore, giving rise to an instability in shoreline shape that can generate different types of naturally occurring coastal landforms, including capes, flying spits, and alongshore sand waves. This instability merely requires that alongshore sediment flux is maximized for a given deepwater wave angle, a maximum that occurs between 35° and 50° for several common alongshore sediment transport formulae. Here we introduce metrics that sum over records of wave data to quantify the long-term stability of wave climates and to investigate how wave climates change along a coast. For Long Point, a flying spit on the north shore of Lake Erie, Canada, wave climate metrics suggest that unstable waves have shaped the spit and, furthermore, that smaller-scale alongshore sand waves occur along the spit at the same locations where the wave climate becomes unstable. A shoreline aligned along the trend of the Carolina Capes, United States, would be dominated by high-angle waves; numerical simulations driven by a comparable wave climate develop a similarly shaped cuspate coast. Local wave climates along these simulated capes and the Carolina Capes show similar trends: Shoreline reorientation and shadowing from neighboring capes causes most of the coast to experience locally stable wave climates despite regional instability.

Citation: Ashton, A. D., and A. B. Murray (2006), High-angle wave instability and emergent shoreline shapes: 2. Wave climate analysis and comparisons to nature, *J. Geophys. Res.*, *111*, F04012, doi:10.1029/2005JF000423.

1. Introduction

[2] Previous work [*Ashton and Murray*, 2006; *Ashton et al.*, 2001] demonstrated that when the angle between wave crests and a shoreline ("wave angle", Figure 1) exceeds the one that maximizes alongshore sediment transport, shoreline planform evolution will be unstable; perturbations to a straight coast will grow, and not flatten as traditionally thought. Discriminating only between waves approaching at angles greater than or less than this maximizing angle ("high" and "low" angles, respectively), numerical simulations predicted that wave climates with a majority of high-angle waves cause surprisingly complex shoreline evolution, resulting in features resembling several different naturally occurring coastal landforms, including capes, flying spits, and alongshore sand waves [*Ashton and Murray*, 2006].

[3] Here we further investigate the relevance of this high wave angle instability along natural shorelines. First, we show that many different formulations for alongshore sed-

iment transport all predict the high wave angle instability. Methods are then introduced to compute more precisely the degree of imbalance between stable and unstable waves in long-term records of wave conditions. These wave climate metrics are computed for wave data along several natural coastlines to determine if present wave climates are consistent with the hypothesis that a predominance of high-angle waves is responsible for the appearance and maintenance of certain types of coastal features such as cuspate spits, alongshore sand waves, and cuspate coasts. Comparisons between model predictions and the way local wave climates change along Long Point, Lake Erie, Canada, and the Carolina Capes, USA, suggest that features of these natural coasts may have been shaped largely by the interactions represented in the model.

2. Comparing Different Sediment Transport Formulations

[4] *Ashton et al.* [2001] demonstrate that a basic instability in shoreline shape follows from the presence of a maximum in the relationship between alongshore sediment flux and deepwater approach angle. For example, the common "CERC" formula [*Komar*, 1971; *Komar and Inman*, 1970; *Rosati et al.*, 2002] predicts that a coastline is unstable whenever deepwater waves approach at angles greater than approximately 42° [*Ashton et al.*, 2001]. Many other formulae, both theoretical and empirical, exist that

---

[1]Division of Earth and Ocean Sciences, Nicholas School of the Environment and Earth Sciences and Center for Nonlinear and Complex Systems, Duke University, Durham, North Carolina, USA.

[2]Now at Department of Geology and Geophysics, Woods Hole Oceanographic Institution, Woods Hole, Massachusetts, USA.
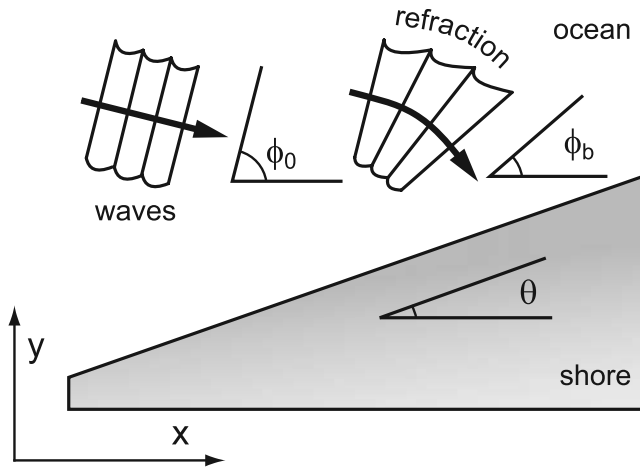
Figure 1. Depiction of terms and axes, demonstrating the orientation of deepwater waves (ϕ_0), refracted breaking waves (ϕ_b), and the shoreline (θ).

relate wave-driven alongshore sediment flux to wave characteristics such as height, angle, and period. Here we look briefly at some of these relationships to determine whether the maximum in sediment transport, or its occurrence around a deepwater angle of 45°, is unique to the CERC formula, or if other relationships also exhibit an easily exceeded deepwater maximum.

2.1. Sediment Transport Relationships

[5] Amongst the large number of formulations for breaking-wave-driven alongshore sediment transport that have been presented in the literature, we have selected several that are frequently referred to, have different derivations, and offer significantly different functional predictions. Besides the semiempirical CERC formula, we will also investigate the (semi) empirical *Kamphuis* [1991] formula with laboratory fit parameters, the analytically derived *Bailard* [1984] formula, and the *Deigaard et al.* [1988] formula developed using detailed numerical modeling (Table 1). For illustration purposes only, we also analyze a hypothetical formula that is similar to the CERC relationship, but lacking a breaking wave maximum in sediment flux.

[6] Alongshore sediment transport relationships can typically be separated into a portion functionally dependant on

wave height (H) and angle ($\phi - \theta$) (Figure 1) and another portion related to sediment characteristics and surf zone geometry (Table 1). The typically empirical proportionality constants, which relate wave inputs to volumetric quantities of alongshore sediment flux (Q_s, m³/s deposited volume), can vary dramatically between different locations and between these formulae. However, although differences in these proportionality coefficients affect the predicted rates of sediment flux (and subsequent shoreline evolution), they do not reflect how Q_s changes as input wave characteristics vary. Accordingly, we compare these sediment transport formulae by normalizing their proportionality constants and looking at them only in terms of their dependence on wave height, angle, and period.

2.2. Comparison of Sediment Transport Formulations

[7] With the exception of the "hypothetical" formula and the Deigaard formula (which is defined for deepwater wave angles), all of these relations show a maximum in Q_s for waves with breaking angles ($\phi_b - \theta$) of 45° if breaking wave height (H_b) is held constant (Figure 2a). Because of refraction, such large breaking wave angles are unlikely for typical wave conditions. However, this does not mean that the high wave angle instability is unlikely to occur. Both H_b and the breaking wave angle (ϕ_b) respond to changes in the shoreline orientation (θ), and neither H_b nor ϕ_b can be assumed constant along an undulating shoreline (Figure 3).

[8] Gradients in alongshore sediment transport are most easily understood using the only wave characteristics that are constant along an undulating coastline: deepwater wave height (H_0) and crest orientation (ϕ_0) (also discussed by *Ashton and Murray* [2006]). Plotting Q_s versus deepwater angles ($\phi_0 - \theta$) shows that, depending on the formula, Q_s is maximized for some angle between 35° and 50° for 2 m, 10 s waves (Figure 2b); all of these equations predict shoreline instability for around half of all possible deepwater approach angles.

[9] Even the hypothetical formula with no breaking wave maximum shows a deepwater maximum almost identical to that of the CERC formula. This similarity is at first surprising. However, the hypothetical formula can be derived from the CERC equation using a small angle approximation that is appropriate for the typically small breaking wave angles. How does a deepwater maximum arise in the absence of a breaking wave maximum? Increasing breaking

Table 1. Investigated Sediment Transport Formulations and Corresponding Maximizing Angles for Breaking and Deepwater Waves[a]

| | | Maximizing Angle | |
Name	Formula	($\phi_b - \theta$)	($\phi_0 - \theta$)
CERC	$Q_s = \left[\frac{K\rho g^{\frac{1}{2}}}{(\rho_s - \rho)(1-p)} \right] H_b^{\frac{5}{2}} \cos(\phi_b - \theta)\sin(\phi_b - \theta)_b$	45°	42°
Kamphuis	$Q_s = (2.27 m^{0.75}\, d_{50}^{-0.25}\, T^{1.5}) H_b^2 \cos^{0.6}(\phi_b - \theta)\sin^{0.6}(\phi_b - \theta)$	45°	34°
Bailard	$Q_s = [0.05 + 2.6 \sin^2 2(\phi_b - \theta) + \frac{0.007 u_{mb}}{W}] H^{5/2} \cos(\phi_b - \theta)\sin(\phi_b - \theta)$	45°	52°
Deigaard	$\frac{Q_s}{Q_{s,max}} = (\sin\ \{2(\phi_0 - \theta)[1 - 0.4\frac{(\phi_0 - \theta)}{90°}(1 - \frac{(\phi_0 - \theta)}{90°})]\})^{5/2}$	N/A	50°
Hypothetical	$Q_s = C_{Hyp} H_b^{5/2}(\phi_b - \theta)$	90	46°

[a]Variables: Q_s, m³/s deposited volume; K, empirical constant (typically 0.7); ρ_s, sediment density (typically 2.65 g/cm³ for quartz density sand); ρ, water density (typically 1.04 g/cm³ for salt water); p, sediment porosity (typically 0.4); g, the acceleration of gravity (m/s²); T, wave period, (s); d_{50}, median grain size (mm); m, beach slope; u_{mb}, maximum oscillatory velocity at breaking (cm/s); W, sediment fall velocity (cm/s).
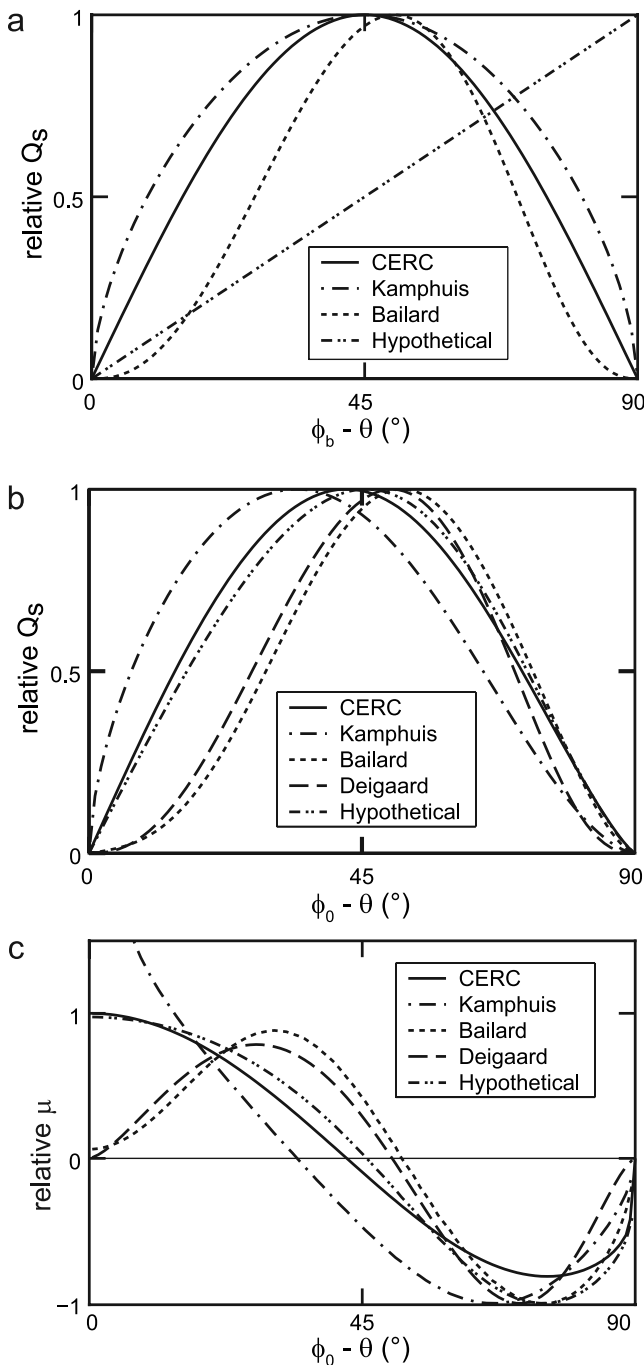
Figure 2. Relative alongshore sediment transport versus (a) breaking wave angle and (b) deepwater wave angle, along with (c) relative diffusivity versus deepwater wave angle. In Figure 2c, positive diffusivities indicate a stable coast; negative values indicate an unstable coast. Deepwater plots were computed by iteratively refracting 2 m, 10 s deepwater waves over shore-parallel contours, using linear wave theory, until depth-limited breaking occurs. Although the relationships in Figures 2b and 2c depend on wave steepness (H_0/T), different "realistic" input wave characteristics do not provide significantly different predictions.

wave angles tend to increase Q_s in the hypothetical formula (and in the CERC equation for breaking wave angles smaller than 45°). However, as breaking wave angles increase, so does the amount of refraction. This refraction stretches wave crests, reducing wave heights, in turn tending to reduce Q_s. As deepwater wave angles increase, the tendency for Q_s to decrease because of decreasing breaking wave heights eventually overwhelms the tendency for Q_s to increase due to increased breaking wave angles (Figure 3). Using the hypothetical formula for typical swells, the resulting transport maximum occurs for swells breaking around 14°, coming from 43° in deep water, similar to the values predicted using the CERC formula (Figure 2) [*Ashton and Murray*, 2006]. The hypothetical formula demonstrates that the deepwater maximum for Q_s required for shoreline instability stems mostly from energy conservation and Snell's law (assuming refraction and shoaling over shore-parallel contours), and not from a breaking angle maximum.
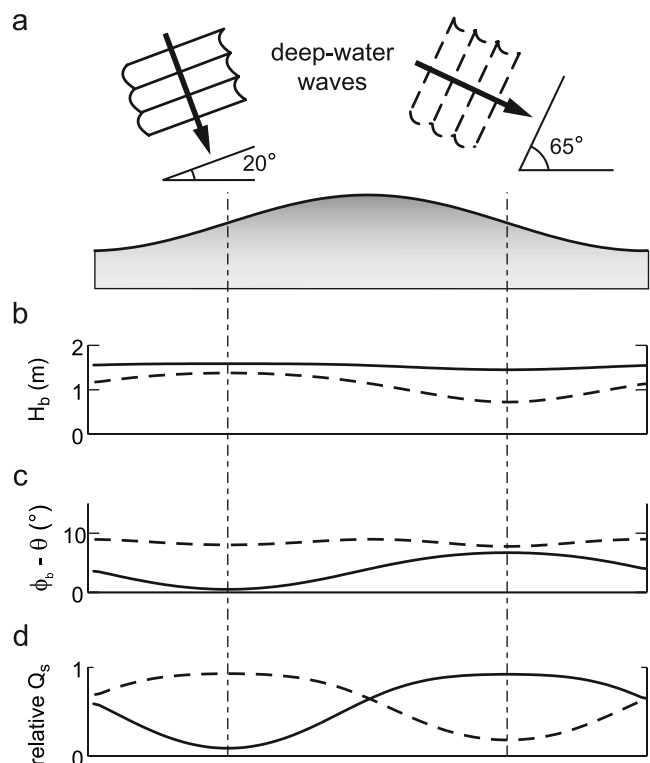

Figure 3. Variation in breaking wave angle and height along an undulating shoreline, with resulting relative alongshore sediment transport. Shown are (a) a nonexaggerated depiction of a shoreline with deepwater waves approaching from low angles (20°) and from high angles (65°), (b) breaking wave height (H_b), (c) relative breaking wave angle ($\phi_b - \theta$), and (d) relative sediment transport (Q_s) along the shoreline. Solid lines (dashed lines) indicate low-angle (high-angle) waves. Note that for low-angle waves, Q_s responds chiefly to changes in breaking wave angle. However, for high-angle waves, wave angles remain almost constant, while breaking wave height varies, resulting in the opposite trend in Q_s. All values were computed for $H_0 = 1$ m, $T = 10$ s, neglecting the bathymetric focusing of wave rays.

[10] Despite the robust presence of a deepwater maximum in alongshore sediment transport, the shapes of the various curves (Figure 2b) and the location of their maxima are not the same, and these formulae would predict somewhat different shoreline responses for waves approaching from the same angles. These differences can better be understood by looking directly at how shoreline evolution depends on wave angle.

2.3. Coastal Evolution and Shoreline Diffusivity

[11] Assuming that the shoreface generally preserves an equilibrium cross-shore shape, and net cross-shore sediment fluxes between the shoreface and deeper water are negligible compared to gradients in alongshore sediment transport, shoreline evolution can be modeled by following a single contour line (e.g., the shoreline) [Pelnard-Consideré, 1956]. With the conservation of mass and the chain rule, this yields

$$\frac{\partial y}{\partial t} = -\frac{1}{D} \frac{\partial Q_s}{\partial x} = -\frac{1}{D} \frac{\partial Q_s}{\partial \theta} \frac{\partial \theta}{\partial x}, \quad (1)$$

where x and y are shoreline coordinates (Figure 1), t is time, and D is the depth of the shoreface. Assuming a reasonably straight shoreline,

$$\frac{\partial \theta}{\partial x} = \frac{\partial^2 y}{\partial x^2}, \quad (2)$$

which, combined with (1), produces a shoreline evolution equation:

$$\frac{\partial y}{\partial t} = -\frac{1}{D} \frac{\partial Q_s}{\partial \theta} \frac{\partial^2 y}{\partial x^2}, \quad (3)$$

a diffusion equation where the diffusivity, μ, varies with the wave angle,

$$\mu = -\frac{1}{D} \frac{\partial Q_s}{\partial \theta}. \quad (4)$$

[12] Numerically differentiating the selected relationships for Q_s accentuates some of the differences between the formulae (Figure 2c). As defined, positive diffusivity represents shoreline smoothing (stability), and negative diffusivity represents growth of shoreline perturbations (instability). The relative magnitudes of the diffusivities are also important, representing how much smoothing or perturbation growth would be associated with waves approaching from a given angle over a given period of time. Not only do all of the relationships show a region of negative diffusivity, they all suggest that instability occurs for approximately half of all possible wave angles with magnitudes of the negative diffusivity comparable to the magnitudes of the positive diffusivity.

[13] Interestingly, most of these relationships suggest that gradients in Q_s along an undulating shoreline are smallest when Q_s is large, and shoreline change should be maximized when Q_s is at a relative minimum (Figure 2b and 2c). Waves coming straight onshore or at particularly large oblique angles should have the greatest effect on planform coastal evolution, despite the relatively small amounts of alongshore sediment transport associated with these waves.

The Deigaard and Bailard formulas offer significantly different predictions than the others by suggesting that diffusivity approaches zero when waves approach directly onshore, a phenomenon would substantially reduce the ability for low-angle waves to flatten a shoreline.

3. Wave Climate Analysis

[14] A diffusivity which varies in both magnitude and sign as wave angle changes suggests that, in nature, a coast should undergo periods of stable (diffusive) and unstable (antidiffusive) evolution over time. Wave angles and heights tend to change over temporal scales of hours to days, whereas appreciable, large-scale shoreline evolution due to sediment flux gradients accumulates over intervals of years, decades, and longer, integrating the effects of storms and seasonal fluctuations. Just as records of waves spanning years to decades can be added up to compute long-term net sediment transport trends, long-term shoreline stability can also be computed from historical wave data.

3.1. Historical Wave Data

[15] Historical wave records represent either measurements or computed values such as Wave Information Study (WIS) hindcast data. Natural wavefields are usually composed of a complex mixture of wave trains with distributions of directions, periods, and heights. Reported wave values, however, typically consist of simplified wave statistics such as "significant" wave height (average of highest 1/3 of measured waves) and the period and direction of the most energetic waves, all of which are averaged over some sampling interval, Δt. Because these data sets span decades' worth of wave events, typically taken at hourly intervals, they provide unique high-resolution archives of long-term wave climates.

[16] WIS hindcasting depends on basin-wide historic meteorological data to generate spectral wavefields which are subsequently propagated and shoaled to determine expected wave values at selected locations, or "stations" [Resio, 1981; Hubertz, 1992] (WIS data are available at http://www.frf.usace.army.mil/wis/wis_main.html). Just like measurements, the values computed at a hindcast station are influenced by the local water depth. There are relatively few locations where long-term wave climates have been measured by buoys. However, because a hindcast station can occupy any arbitrary location, a dense network of WIS stations blankets the U.S. coastline, providing data that are particularly useful for comparative wave-climate analyses.

3.2. Contributions to Diffusivity

[17] Every approaching wave causes some alongshore sediment transport, and subsequently contributes to the evolution of the coastline, either diffusively or antidiffusively. The sum of these individual diffusivity contributions, μ_i, provides a net diffusivity, μ_{net}:

$$\mu_{net} = \frac{\sum_{i=1}^{n} \mu_i \Delta t_i}{\sum_{i=1}^{n} \Delta t_i}, \quad (5)$$

where n is the number of data points. With units of m/s^2, μ_{net} will be positive for stable coasts and negative for

unstable coasts. A dimensionless "instability index", Γ, assesses the competition between diffusion and antidiffusion:

$$\Gamma = \frac{\sum_{i=1}^{n} \mu_i \Delta t_i}{\sum_{i=1}^{n} |\mu_i| \Delta t_i},$$ (6)

and ranges between 1 for a wholly low-angle climate and -1 for a wholly high-angle climate. An Γ of zero would mean that a wave climate is on the verge of instability: Low- and high-angle waves balance each other out. Note that while the instability index represents the "competition" between high- and low-angle waves, because it is normalized it does not provide information on the magnitude of diffusion or antidiffusion; if a coast with a large Γ generally experiences small waves, its resultant μ_{net} could be smaller than that of a coast with a smaller Γ, but larger waves.

[18] Recasting the CERC formula in terms of deepwater waves, assuming waves refract over shore-parallel contours, provides [*Ashton and Murray*, 2006]:

$$Q_s = K_2 T^{1/5} H_0^{12/5} \cos^{6/5}(\phi_0 - \theta) \sin(\phi_0 - \theta),$$ (7)

where K_2 typically equals ~ 0.34 m$^{3/5}$s$^{-6/5}$ for root-mean-square (energy averaged) wave height values, $H_{0,rms}$, and ~ 0.15 m$^{3/5}$s$^{-6/5}$ for significant wave heights, $H_{0,S}$ (assuming $H_{0,S} \approx 1.4 H_{0,rms}$ [*Fredsoe and Deigaard*, 1992; *Komar*, 1998]).

[19] Inserting (7) into (4) yields

$$\mu = \frac{K_2}{D} T^{1/5} H_0^{12/5} \left\{ \cos^{1/5}(\phi_0 - \theta) \left[\left(\frac{6}{5}\right) \sin^2(\phi_0 - \theta) \right. \right.$$
$$\left. \left. - \cos^2(\phi_0 - \theta) \right] \right\}.$$ (8)

[20] Disregarding the constants, K_2 and D, which do not vary as wave characteristics change, (8) can be split into two parts, with one part representing the contribution wave height (and to a small degree, wave period) has on potential alongshore sediment transport (and subsequently, μ):

$$E = T^{1/5} H_0^{12/5}.$$ (9)

[21] Conceptually similar to the more common "wave energy" (proportional to H^2), E, the "deepwater wave height contribution to Q_s", more exactly represents how deepwater wave height and period contribute to Q_s based upon the CERC formula. The other part of the diffusivity represents the wave angle effect:

$$\psi = \left\{ \cos^{1/5}(\phi_0 - \theta) \left[\left(\frac{6}{5}\right) \sin^2(\phi_0 - \theta) - \cos^2(\phi_0 - \theta) \right] \right\}.$$ (10)

[22] This second part reflects how a wave's angle influences the magnitude of its contribution to coastal stability or instability, also determining the sign of that influence; ψ is

the source of the negative diffusivity values for high-angle waves (Figure 2c).

[23] Because of its common use, we will most often use the CERC formula. However, other formulae can be similarly split into E and ψ components, and we will also investigate the sensitivity of computed wave metrics using the Kamphuis and the Deigaard formulae, which have different angle dependence (Figure 2) and scaling for E. Derivation of deepwater formulae for these relationships is summarized in Appendix A.

3.3. Sample Computation: North Carolina Outer Banks

[24] To provide a concrete example, we will analyze the wave climate for the shoreline around the U.S. Army Corps of Engineers' Field Research Facility (FRF), located in Duck, North Carolina, United States, along the Outer Banks barrier island chain (Figure 4). Atlantic WIS station 255, located offshore of the FRF at a depth of 164 m, past the continental shelf, provides deepwater data values suited for diffusivity computations (Figure 4). Hourly data summaries at this station cover 1980–1999, reporting significant wave heights and average (energy-weighted average over all frequencies) and peak (average at peak energy frequency) values for wave period and approach angle. Because of the weak dependence upon wave period, using peak versus average wave period does not significantly affect computed values; however, the difference between using peak instead of average approach angles can be significant (as explored below).

[25] Multiplying E by ψ for each recorded wave value provides values for μ that can be summed and normalized to compute Γ (Figure 5) (normalization eliminates the D and K_2 terms). For a coast with the orientation of the FRF (shore-perpendicular direction of 72°, Figure 4), data from WIS station 255 suggest $\Gamma = 0.02$, a marginally stable climate. The generally smooth coast in the vicinity of the FRF region lacks obvious large-scale rhythmic features, as expected for a low-angle shoreline with $\Gamma > 0$. This computation also suggests that although low-angle waves dominate, high-angle waves are not uncommon at the FRF, representing 49% of the wave contribution to shoreline evolution.

3.4. Diffusivity as Coastal Orientation Changes

[26] How stable would a coast with a different orientation be at this location? Given a deepwater wave record, Γ can be computed for any arbitrary shoreline orientation. Rotating though different angles, Γ changes through its dependence on the "angle effect" term in (8). Rotating the shore also introduces a new "window" of high-angle waves that did not approach a shoreline of the previous orientation. This could result in changes in Γ that would be impossible to predict using only local measurements at one coast, as a nearby shore with even a slightly different orientation would experience a window of (strongly antidiffusive) waves not experienced by the coast where the measurements were taken.

[27] A "stability plot", representing the wave climate for different hypothetical shoreline orientations, depicts how Γ changes as a coast is rotated (Figure 6). At the location of the FRF, a coast with an orientation pointing in a more
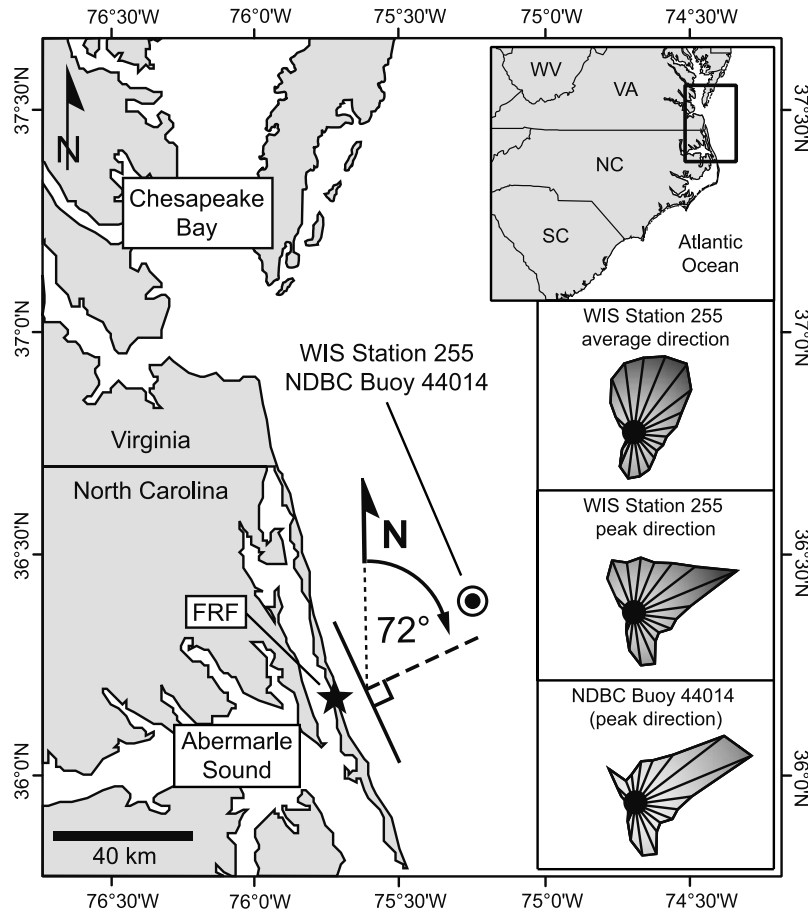
Figure 4. Location map of North Carolina Outer Banks and the FRF. Insets show wave roses of binned sums of E for WIS station 255 (average direction, peak direction) and NDBC buoy 44014 (approximate location of both stations indicated by the double circle). Also shown is the axis definition used for shore orientations of natural coasts: A line perpendicular to the coastal trend at the FRF projects toward 72° east of north.

northerly direction (rotated counterclockwise) would be more stable than a coast with the FRF shoreline's orientation (Figure 6a). Correspondingly, data from WIS station 255 suggest that a coast with a more easterly orientation (rotated clockwise) would be less stable, and furthermore that a coast with only a slightly different orientation would be unstable. Despite the differences between their specific predictions for μ (Figure 2c), both the Kamphuis and the Deigaard formulae also predict a marginally stable wave climate for orientations similar to the FRF ($\Gamma = 0.10$ and 0.01 for the Kamphuis and Deigaard formulae, respectively), with almost identical changes in Γ rotating through different hypothetical shoreline orientations (Figure 6a).

[28] These stability plots bear a resemblance to the "littoral drift roses" presented by *Walton and Dean* [1973; *Rosati et al.*, 2002; *Dean and Dalrymple*, 2002], which were also used to present a shoreline instability that is essentially a subset of the high wave angle instability (although there are key distinctions, as discussed in Appendix B).

3.5. Cautions for Computing Stability Metrics

[29] Q_s is nearly conserved during wave refraction, in the sense that if either deepwater or intermediate-water wave

values were entered into the breaking wave CERC formula (Table 1), the computed alongshore sediment fluxes would be similar. On the other hand, diffusivity changes significantly if wave values from different depths are considered, and a deepwater location is ideal for measurements used to compute diffusivity; slight reductions of the angle of the most high-angle waves (caused by refraction) dramatically reduces their computed contribution to instability (Figure 2c).

[30] However, if data is collected too far offshore, it might not necessarily represent the conditions at the coast; for example, data from an offshore location might not include the contribution of frictional dissipation across the shelf or the local generation of waves felt at the coast. Wave dissipation could be particularly pronounced for swell (long period) waves approaching from the most oblique angles [*Ardhuin et al.*, 2003], correspondingly increasing the importance of local winds in contributing high-angle wave energy from the most oblique angles. Also, if long-period waves refract across a shelf with contours that differ significantly from coast-parallel, measurements taken so far offshore that all the waves are fully deepwater will not accurately reflect the wave climate where the waves first
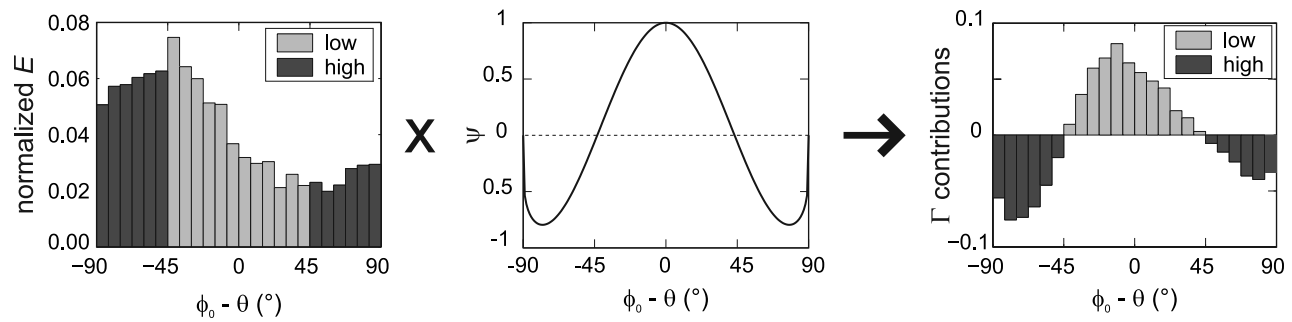
Figure 5. Wave climate instability computation for the FRF, computed using data from WIS station 255 from 1980 to 1999 by multiplying the binned "energy" (E) values by the "angle effect" (ψ). The resulting values are summed and normalized, resulting in Γ of 0.02. (Note: figures are a visualization aid, the actual metrics are computed by summing μ contributions for each wave data point per (6), not by multiplying the binned data).

encounter shore-parallel contours (e.g., the seaward edge of the shoreface).

[31] Therefore an ideal wave data collocation station for computing the stability of the local shoreline trend is close to the shore, but in deep water. As a situation with such a steep shelf is rare (particularly for generally sedimentary coasts), data often are collected at a location of intermediate depth, where short-period (storm) waves are deepwater waves and long-period (swell) waves are at an intermediate depth (and therefore poorly defined by both shallow and deepwater wave approximations utilized in deriving (7)). Data from such a station could either be back refracted to deepwater values assuming parallel shelf contours or entered into (8) as if they represented deepwater quantities. This second approach effectively assumes that refraction up to the station was over non-shore-parallel contours, but subsequent refraction will be over shore-parallel contours.

[32] Computed metrics also depend on the input data. The National Oceanic and Atmospheric Administration's National Data Buoy Center (NDBC) buoy 44014, located close to the position of WIS station 255, has hourly records of significant wave heights and peak angles from 1993 to 2003 at a location with a water depth of 48 m (Figure 4). (NDBC data are available at http://www.ndbc.noaa.gov/index.shtml.) Although some Atlantic swell waves have begun to shoal at this depth, computations show identical wave metrics for both measured and back-refracted values; this station can be considered "deepwater" for the purposes of computing the wave climate metrics presented here. The NDBC buoy 44014 wave climate visibly differs from the hindcast WIS station 255 climate (Figure 4); however, the NDBC buoy data report peak wave directions, and this measured climate should be compared with one derived from the WIS peak direction data. The peak angle data match more closely (Figure 4). In contrast with the WIS average direction data, both the WIS peak and the NBDC buoy data suggest a dominantly stable wave climate, with Γ of 0.24 and 0.33, respectively, for the FRF orientation (Figure 6b). (Although the two records span different time intervals, the overlapping data demonstrate the same relationship). Because the NDBC data are based on measurements, not calculated values hindcast from meteorological readings, they would usually be considered superior to WIS hindcast values. However, as average wave direction rep-

resents the energy-averaged contributions to alongshore sediment flux (approximately averaging over E components), average direction data are best suited for computing Γ. On the other hand, the similarity of the peak WIS and the NDBC climates suggests that the hindcast at this location correlates reasonably well with the measured wave climate (as represented by the simple wave statistics).

[33] Yet another set of usable wave climate measurements exists for this location, taken by a Waverider buoy 4 km offshore of the FRF at a depth of approximately 17 m, with records of H_{rms}, peak wave period, and peak wave direction. (FRF data are available at http://www.frf.usace.army.mil/.) Back-refracting data spanning November 1996–2003 taken at this intermediate-depth location provides deepwater values that suggest an even more stable climate than the WIS and NDBC data do, with $\Gamma = 0.55$. Because of the Waverider's proximity to the shore, it only records waves approaching at $\pm 90°$ to the orientation of the shoreline at the FRF, and contains no information about waves within the new high-angle "window" that would approach a coast with a different orientation. Although data measured this close to shore can be used to compute local stabilities, they cannot be used to develop wave stability plots as in Figure 6b.

[34] Along a natural coast, there will always remain a degree of imprecision in these computed wave metrics, due not only to the variability between the alongshore sediment transport formulae, but also because much information is lost when calculating simple wave statistics. Peak directions neglect the rest of the wave spectrum which could contain less energetic components that could also contribute to alongshore sediment transport. Average wave direction values lump together a wide range of approaching waves, and the angle dependence of diffusivity suggests that the combined effects on diffusivity could be significantly different from that of a wave energy average. However, because average wave directions retain information about more of the wave spectrum than peak values do, computations used in the rest of this paper will whenever possible be based upon average wave directions (along with significant wave heights and average period). The sample computations for the coast around the FRF demonstrate this variability. However, all of the wave climate analyses suggest that the local FRF wave climate is a stable one,
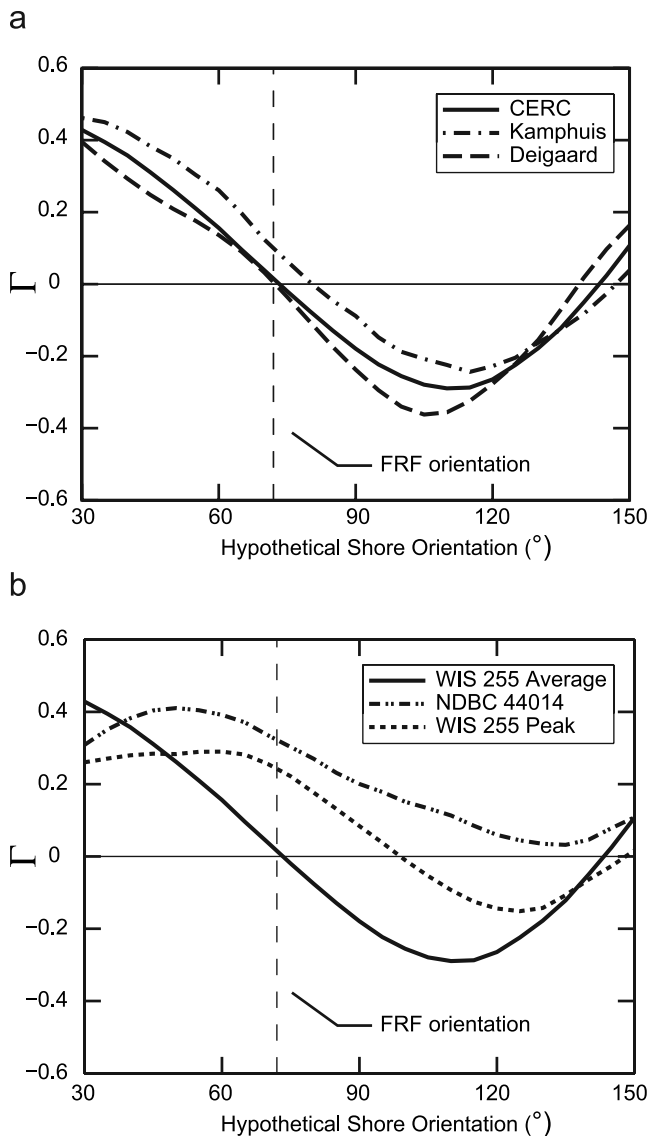
a

b

Figure 6. Values of Γ for shorelines of hypothetical orientations for (a) average direction values at WIS station 255 for different sediment transport formulae and (b) for the CERC formula using average direction and peak direction both at WIS station 255 and peak direction at NDBC buoy 44014. At each orientation (moving in 5° increments), *Inst* is calculated by summing μ contributions from the entire data record.

also showing similar trends in Γ for different coastal orientations.

4. Model Predictions and Natural Wave Climates

4.1. Wave Climates Along a Flying Spit: Long Point

[35] Long Point is a flying, or "cuspate" spit along the northern shore of Lake Erie, in Ontario, Canada, projecting approximately 30 km into the lake (Figure 7). Formed over the Holocene, this spit has elongated and migrated downdrift (to the east) to its current location [*Coakley*, 1992], and the wave-dominated lake-facing shore continues to experience frequent overwash [*Davidson-Arnott and Reid*, 1994].

Probably because it began as a large glacial moraine acting as a perturbation to the shoreline trend [*Coakley*, 1992], Long Point is not part of a chain of spits, unlike some other flying spits (such as those found along the Ukrainian [*Zenkovich*, 1959; *Ashton et al.*, 2001] and Russian coasts [*Zenkovich*, 1967; *Ashton and Murray*, 2006]).

4.1.1. Wave Climate

[36] Because elongate water bodies have large fetches along their main axis, high-angle waves should be common along their long axis coasts, a phenomenon enhanced at Lake Erie by dominant westerly winds [*Stewart and Davidson-Arnott*, 1988]. Consequently, Lake Erie experiences a unimodal wave distribution with almost all of the wave energy approaching from the west, as shown by WIS hindcast covering 1956–1987 from Lake Erie WIS station 33 (Figure 8). Hindcast for the Great Lakes are recorded at 3-hour intervals, providing significant wave height, peak wave period, and peak wave direction. Although using peak, instead of average, wave directions resulted in significantly different stability predictions for the FRF, the unimodal nature of Lake Erie's wave climate decreases the likelihood that average wave directions would significantly differ from peak wave directions. The WIS data set represents the only relatively long-term, high-resolution estimate of wave conditions available at this location (directional measurements, from nearby NDBC buoy 45012, only extend back to 2002).

[37] Stability computations show that along Long Point, local wave climates are unstable at either end of the spit, and marginally stable in between (Figure 8). This pattern is consistent with the prediction [*Ashton and Murray*, 2006] that a single shoreline bump responds to high-angle waves by extending offshore as a flying spit until the central shoreline approaches an angle where high- and low-angle waves tend to balance, with high-angle wave dominance at the proximal and distal ends of the spit.

[38] *Ashton and Murray* [2006, Figure 9] present a stability diagram developed from numerical simulations describes how wave climate characteristics influence the form of emergent high wave angle features (Figure 9). Although the model variable U, the fractional amount of high-angle waves, does not exactly correspond with Γ, and citing the potential inaccuracies computing Γ discussed above (Section 3.5), we can make rough comparisons between the two to see where the natural wave climates at Long Point lie within the stability diagram. Because there is no clearly defined shoreline trend from which Long Point extends, it is not straightforward how to compare the measured wave climate for this flying spit with the model parameters. However, the orientation of the shoreline along the spit produces an estimated minimum value of $\Gamma = -0.4$ at the updrift end of the spit (Figure 8), which corresponds to $U \sim 0.7$. For extremely asymmetric wave climates (such as the one Long Point experiences), this value lies within the parameter space producing flying spits (Figure 9).

4.1.2. Alongshore Sand Waves: Observations

[39] *Stewart and Davidson-Arnott* [1988] and *Davidson-Arnott and Van Heyningen* [2003] discuss another type of large-scale coastal phenomenon occurring along Long Point: superimposed on this single spit shape are smaller coastal features referred to as "alongshore sand waves" (or
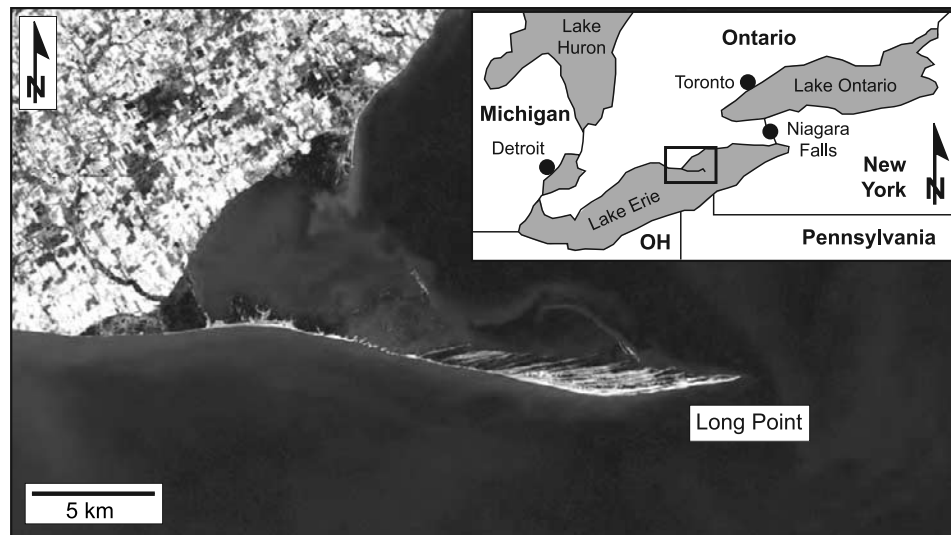
Figure 7. Long Point, Lake Erie, Canada. Data are available from USGS/EROS, Sioux Falls, South Dakota; source for this data set was the Global Land Cover Facility (http://www.landcover.org).

"longshore sandwaves"), in this case kilometer-length plan view humps with cross-shore amplitudes on the order of 100 m that migrate alongshore toward the east, in the direction of net sediment transport. These sand waves occasionally merge as they migrate alongshore, are more pronounced at their downdrift end, and as their alongshore length increases, so does their cross-shore extent. In many ways, these features, which have alongshore scales much larger than the surf zone, share behaviors with simulated "alongshore sand waves" shown by *Ashton et al.* [2001] and *Ashton and Murray* [2006] to form under the influence of high-angle waves.

[40] Sand waves tend to exist at two locations along Long Point, in the nook at the proximal end of the spit, and along the distal end, where the coast again changes its orientation [*Stewart and Davidson-Arnott*, 1988]. The zones where Γ is negative overlap with the sand wave regions: High-angle waves dominate where the sand waves are found (Figure 8). This correspondence suggests that the high wave angle instability and interactions similar to those in the model could be responsible for the observed sand wave behavior.

4.1.3. Comparisons to Modeled Alongshore Sand Waves

[41] In all simulations where there is a net direction of alongshore sediment transport (asymmetry to the wave climate), high-angle waves cause initially small, migrating sand waves to emerge. If high-angle waves only slightly dominate the wave climate, the features remain sand waves indefinitely [*Ashton and Murray*, 2006, Figure 9]. With greater high-angle dominance, features that remain as sand waves for some time ultimately develop protruding spits, becoming either "reconnecting spits" or "cuspate spits" (Figure 9). For the Long Point sand wave fields, the WIS data suggests that Γ varies between −0.2 and −0.4 (Figure 8b), which would approximate values for *U* ranging between 0.6 and 0.7, suggesting that reconnecting or flying spits should eventually form (Figure 9). Although the Long Point sand waves intermittently develop an emergent bar and landward trough at their downstream ends [*Davidson-*

Arnott and Van Heyningen, 2003], they do not develop into cuspate spits as suggested by the model.

[42] The Long Point sand wave fields (and the corresponding unstable reaches) extend ∼10 km along-shore. With migration rates of ∼100–300 m/year [*Davidson-Arnott and Van Heyningen*, 2003], it is possible that sand waves traverse the unstable coastal region before they attain more pronounced aspect ratios and prominent spits, remaining sand waves even in a wave climate heavily dominated by high-angle waves. Another possibility is that the damping of the instability at the relatively small scales of these sand waves would result in weaker high-angle domi-nance than suggested by our wave climate analysis that assumes refraction takes place over shore-parallel contours [*Falqués and Calvete*, 2005].

[43] The limited alongshore domain can also explain other differences between modeled and observed sand waves. For instance, *Davidson-Arnott and Van Heyningen* [2003] suggest that an important distinction between sand waves observed at Long Point and those simulated by *Ashton et al.* [2001] is that simulated features develop simultaneously along the coast whereas the Long Point sand waves form one by one at the updrift end of each of the sand wave fields. At any moment, modeled sand waves are approximately the same size everywhere, with an alongshore length scale that correlates with their age [*Ashton and Murray*, 2006, Figure 11]. On the other hand, as the observed sand waves migrate downdrift, traversing the field, they tend to merge with one another; in this way, the older sand waves at the downdrift end of the field are older, and tend to be larger than those at the updrift end [*Stewart and Davidson-Arnott*, 1988; *Davidson-Arnott and Van Heyningen*, 2003].

[44] While these differences in development styles may ostensibly seem significant, they do not necessarily imply a significant difference in the processes and interactions, rather, they can be understood as the consequence of different initial and boundary conditions. The model employs periodic boundary conditions, so that the domain
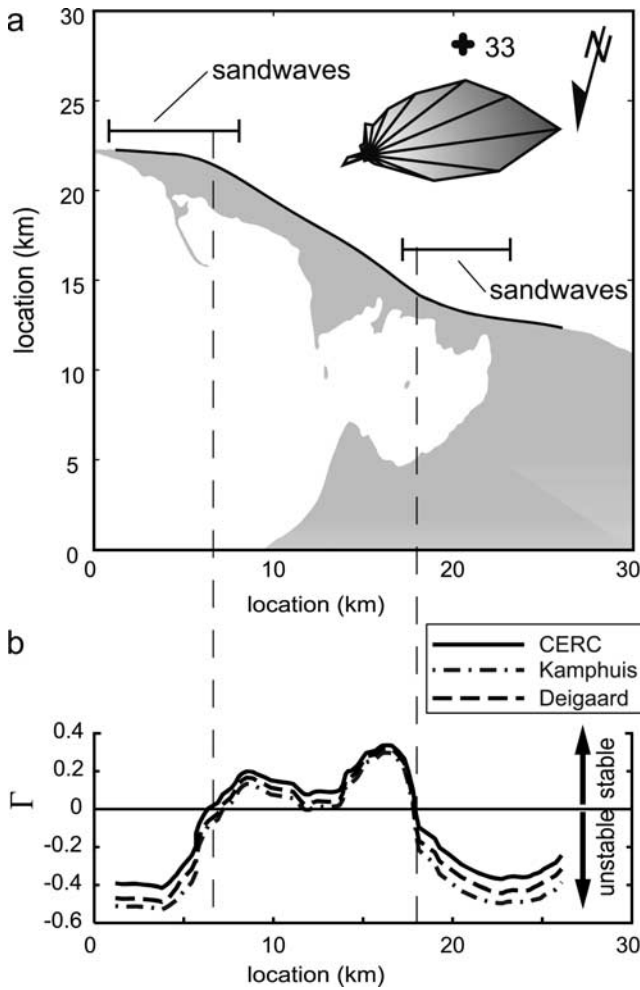
Figure 8. Long Point shoreline and computed Γ values. (a) Long Point shore rotated 195° clockwise, with shoreline accented, including location of WIS station 33 and rose of E values from 1956 to 1995. Hindcast values account for ice cover [*Driver et al.*, 1991]. (b) Corresponding Γ values along the highlighted coast.

tend to diffuse away over the stormy winter season, a phenomenon consistent with computations by *Falqués and Calvete* [2005] indicating that the instability is hampered at small alongshore scales when waves are large and have long periods.) At other sand wave sites, different perturbations appear to initiate sand waves, including episodic inlet openings [*Thevenot and Kraus*, 1995], sediment bypass pulses at inlets [*Ruessink and Jeuken*, 2002], riverine flood deposits [*Inman*, 1987], and even the emplacement of beach fill [*Grove et al.*, 1987]. Although simulations begin with randomly located, small-amplitude perturbations rather than coherent and significant perturbations such as these, the shoreline shapes in the model rapidly ''forget'' the details of the initial perturbations as they continue to self-organize into a sand wavefield. Similarly, once triggered, Long Point sand waves change shape and size as they migrate away, phenomena apparently having little to do with the bar welding that kicks off their formation.

[46] Bar welding represents one of several processes described by *Davidson-Arnott and Van Heyningen* [2003] that transpire at spatial and temporal scales smaller than those resolved in a simple one-line model such as ours which implicitly averages over the myriad bar and channel changes operating over event and seasonal timescales [e.g., *Wright and Short*, 1984; *Lippmann and Holman*, 1990]. For example, *Davidson-Arnott and Van Heyningen* [2003] demonstrate that sand wave migration on Long Point occurs partly through episodic bar welding at the downdrift end of the sand waves. The profiles shown in these reaches, however, suggest that bar emergence coincides with accretion of mass in the profile, indicating a locally positive net sediment balance. At least in this case, the welding of nearshore bars onto the shore could be seen as a manifestation of longer-term shoreface accretion, such as from a convergence of alongshore sediment flux (which is the process that drives the modeled behavior).

[47] Along both the modeled and natural coast, new sand waves do not typically form within existing sand wave fields. Within the numerical model, the self-organization of
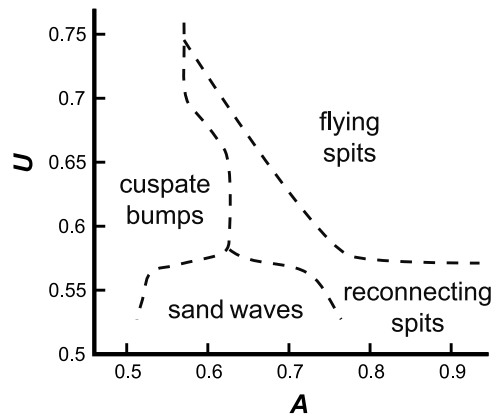
does not feature updrift and downdrift boundaries. Different behavior would occur if the model had prescribed updrift and downdrift boundaries. Starting with an initially straight shoreline (and a wave climate conducive to sand waves), the following sequence would necessarily occur: Sand waves would initially form everywhere. Sand wave migration away from the updrift end of the domain, however, would leave an open space of increasing length. A new sand wave would form there, and subsequently migrate through the domain, possibly merging with its earlier formed neighbors. Once the original sand waves have exited the domain, the simulated sand wave field would be comparable with the Long Point sand waves: all of the remaining sand waves would have formed at the updrift limit, with size and age increasing in the downdrift direction.

4.1.4. Alongshore Sand Wave Formation Mechanisms

[45] There appear to be many mechanisms for sand wave formation. At Long Point, welding of surf zone bars triggers alongshore sand waves. (Sometimes, if bar welding results in nascent sand waves of insufficient size, these features

Figure 9. Phase plot of modeled shoreline shapes with variation of wave climate variables A (proportion of waves from one direction) and U (proportion of unstable, high-angle waves). For quick comparisons, Γ loosely corresponds with $2(0.5 - U)$. Note that the opposite relationship (deriving U from Γ) will only hold for the most simplistic wave climates.
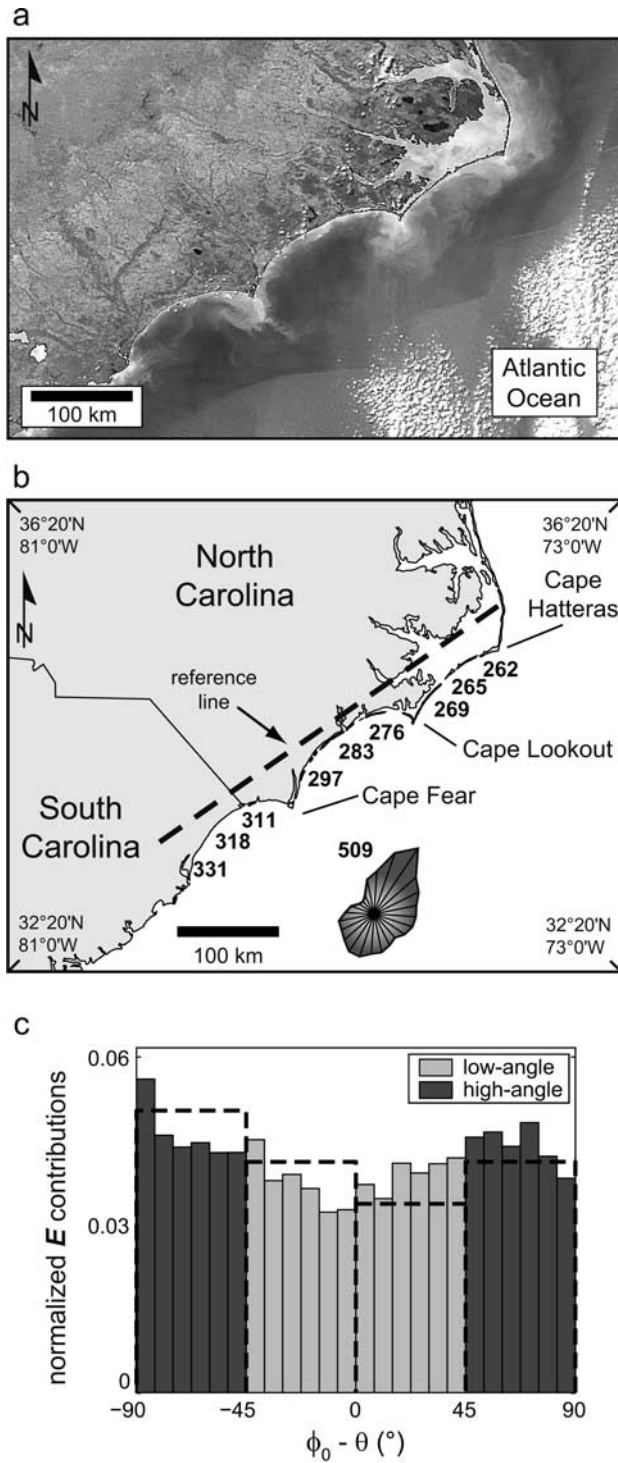
Figure 10. (a) Satellite mosaic and (b) location map of the Carolina Capes, North Carolina and South Carolina, United States, including locations of the WIS stations used in wave climate analyses, rose of tabulated E values for WIS station 509, and the reference line oriented along the cape embayments used to determine (c) the historic wave climate at WIS station 509, fit with the model input wave climate ($U = 0.6$, $A = 0.55$, dashed lines). (Image courtesy of the SeaWiFS Project NASA/GSFC and ORBIMAGE.)

simulated sand wave shapes suggests that the details of the processes that trigger the instability and initially form sand waves are not as significant as the finite amplitude, nonlinear interactions that constitute the sand wave-like behavior [*Werner*, 1999; *van Enckevort et al.*, 2004]. The results of the WIS data analysis, that sand waves appear along the sections of the coast dominated by high-angle waves, suggests that the instability in shoreline shape, and consequent self-organization, likely plays an important role in the observed Long Point sand wave behavior.

4.2. Stability of a Cuspate Coast: The Carolina Capes

[48] The coast of North Carolina, United States, extending into South Carolina, features the "Carolina Capes", cuspate forelands with an approximate wavelength of 125 km and average cross-shore excursion of ∼20 km (Figure 10). *Ashton et al.* [2001] suggest that a predominance of high-angle waves may be responsible for the formation and maintenance of these capes. Here we will compare the trends in local coastal stability along both the natural capes and a set of simulated capes generated by a wave climate similar to the natural one, using the new wave climate metrics. Along the Carolina Cape coast, we will analyze just WIS data, as the only directional measurement station along this coast, NBDC buoy 41013, has only collected data since March 2003 and is located close to Frying Pan shoals, a bathymetric high that strongly affects local wavefields.

4.2.1. Stability of the Coastline Trend

[49] First, we test the prediction that high-angle waves currently predominate along this coast, examining the wave climate for a coastline with the regional trend defined by the cape embayments (150°, Figure 10). Fully deepwater values can be used to compute stability metrics because the strike of the continental shelf offshore of the Carolina Capes is subparallel to this regional coastline trend. (Across the continental shelf, waves will propagate over contours with large-scale trends approximately parallel to the coastline trend. This analysis, however, does not account for the dissipation of long-period waves across the shelf, as discussed in section 3.5.) Data from 1980 to 1999 at Atlantic WIS station 509, at a depth of 215 m (Figure 10b) shows that for a coastline trend of 150°, $\Gamma = -0.09$; a straight shoreline with an orientation connecting the cape embayments would be unstable. This agrees with the previous, more qualitative assessment suggesting that high-angle waves dominate along this coast made by *Ashton et al.* [2001], based upon an older WIS data set.

4.2.2. Numerical Simulation of a Cuspate Coast

[50] After establishing that the coastal trend is predominated by high-angle waves, the next question is: does a similar wave climate form comparable cuspate features in the numerical model of *Ashton and Murray* [2006]? The actual Carolina Capes have been influenced by sea level changes and other geologic controls, and moreover consist of barrier islands, not a mainland coast as the model represents (interpreted most literally). In addition, this long stretch of the Carolina coast almost certainly never had a straight configuration that the model simulations start with. Thus this model does not reenact the detailed geological history of the Carolina coast, and this is not our goal. Instead, as we discuss further in section 4.2.5, we are testing whether the active process of wave-driven alongshore
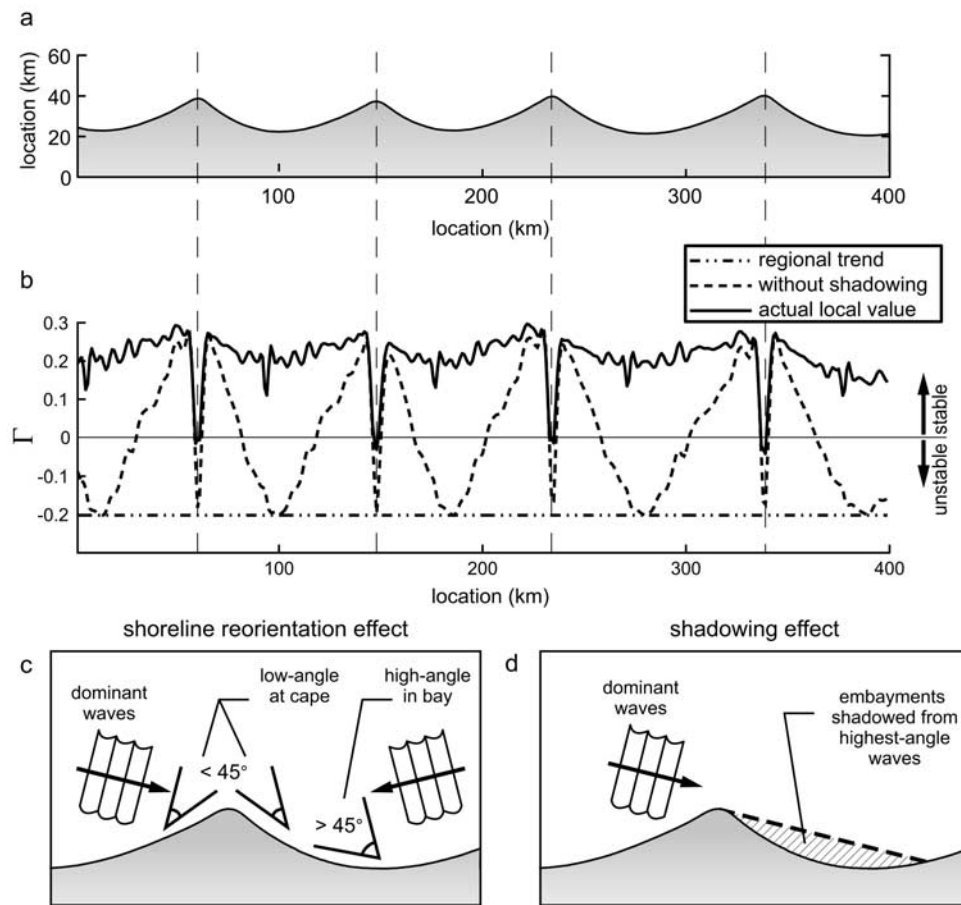
Figure 11. (a) Model shoreline generated by the wave climate shown in Figure 10c, using the same model parameters as those used by *Ashton and Murray* [2006], except cells have a width of 1000 m. (b) Γ along the simulated coast computed for different scenarios. Local shoreline stability is increased through (c) reorientation of the shoreline and (d) shadowing by cape tips.

transport could plausibly have determined important aspects of the present coastline shape.

[51] Simulation wave climate parameters of $U = 0.6$ and $A = 0.55$ loosely match the WIS climate compared to the regional trend, corresponding to $\Gamma \sim -0.20$ (Figure 10c). These values fall within the simulation parameter space that generates ''cuspate coasts'' (Figure 9). Approximately 50,000 simulated years after starting with a straight coastline, with 1.7 m (H_s), 8 s waves, capes attain a similar $\sim$125 km spacing, with $\sim$20 km cross-shore excursions (Figure 11a). Alongshore sediment transport alone can plausibly form cuspate forelands similar to the Carolina Capes, although (as discussed further below in Section 4.2.5) the timescale for forming the capes from a straight coast exceeds that of the most recent sea level highstand.

4.2.3. Local Wave Climates Along a Simulated Coast

[52] Analysis of local wave climates in the model reveals that the simulated coast has self-organized from an initially unstable straight shape into a configuration with locally stable coasts despite a regionally unstable wave climate. Figure 11b shows Γ computed along the cuspate shore, based on the regional wave distribution that generated the coast (e.g., $U = 0.6$, $A = 0.55$). Computations use a cell-based angle (averaged over left and right neighbors) to determine local orientations, and waves shadowed by local neighbors do not contribute to Γ values.

[53] With the exception of the cape tips, computed values for Γ are positive, $\sim$0.2 along the embayments (Figure 11b). This stabilization of local wave climates stems from two basic processes: shoreline reorientation and shadowing by the capes. As a shore rotates, it faces incoming regionally high-angle waves more head-on, reducing their antidiffusive strength (Figure 11c). Although this mechanism increases the stability of the local wave climate along the cape flanks, shore orientations within the embayments remain subparallel to the regional trend, meaning that reorientation alone cannot explain the increased stability along the entire coast. Within an embayment, shadowing by the cape tips protects the shore from the highest-angle waves that contribute the most to shoreline instability (Figure 11d). Neglecting shadowing effects and recomputing Γ, the relative effect of these two processes becomes more clear: without shadowing, the coast within the middle of the embayments would still experience an unstable climate (Figure 11b).

[54] For most of the shoreline of this simulated large-scale cuspate coast, locally stable wave climates prevent the growth of smaller bumps, leading to generally smooth shorelines despite the presence of regional wave-climate instability. The simulated shore self-organizes in a manner
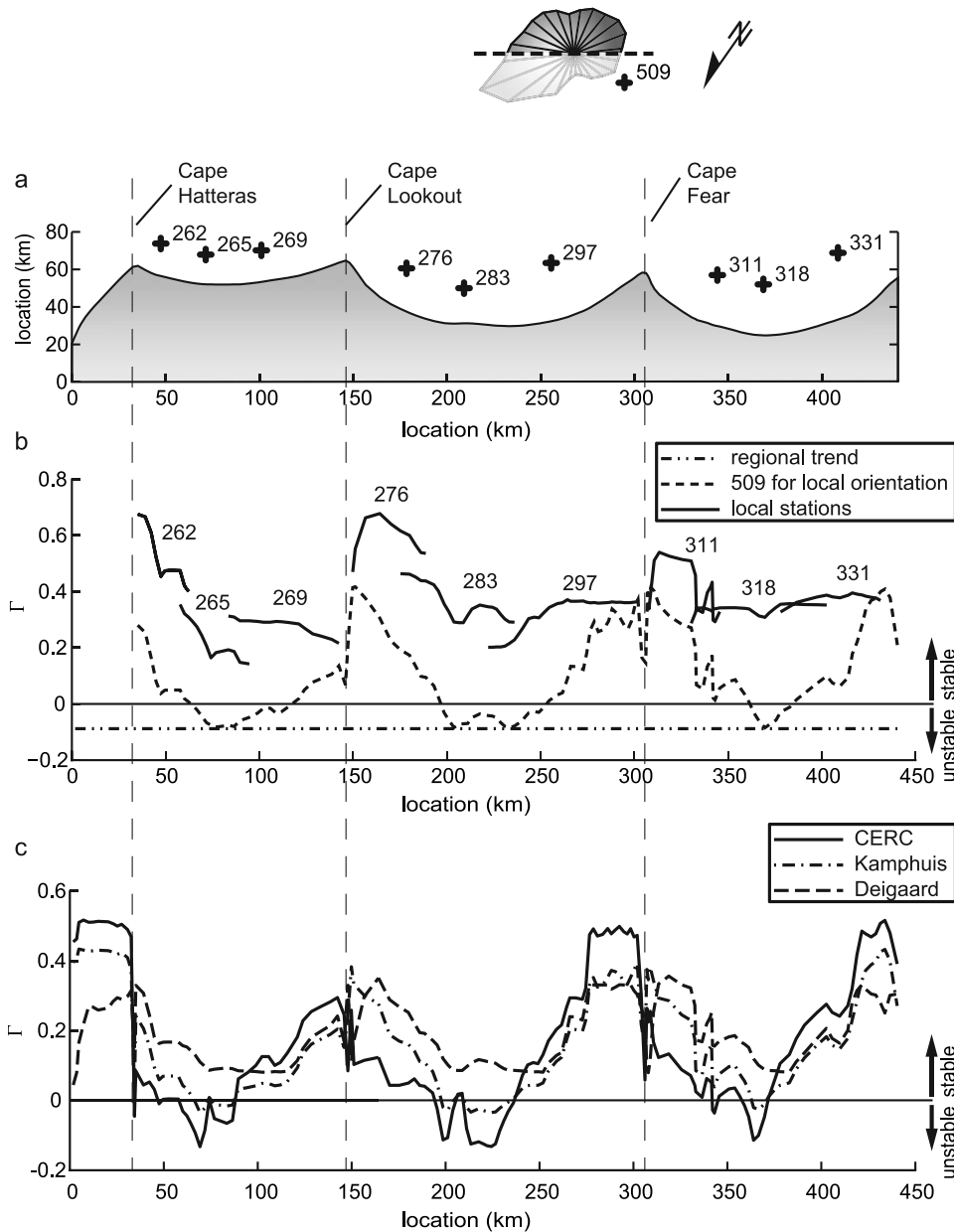
Figure 12. (a) Carolina Capes shoreline rotated about the reference line shown in Figure 10b with the locations of analyzed WIS stations. Also shown is a rose of tabulated E values for WIS station 509 data with rotated reference line (from Figure 10b, dashed line). (b) Γ for local orientations and different WIS data. (c) Comparison of different alongshore sediment transport formulae using WIS station 509 data. Regional wave climates are computed using only waves that approach at $\pm 90°$ to the reference line (corresponding to the opaque portion of the wave rose).

that dampens the growth of new perturbations. As the proportion of high-angle waves increases, aspect ratios (cross-shore extent/alongshore spacing) increase [*Ashton and Murray*, 2006], which would heighten both the reorientation and shadowing effects. Shadowing represents a long-range, nonlocal effect; changes at one cape can influence the evolution of the shoreline along a neighboring, but distant, cape, communicating local changes across large distances.

4.2.4. Local Wave Climates Along the Carolina Capes

[55] Do the Carolina Capes demonstrate wave climate trends similar to the modeled capes? Recomputing Γ for the wave climate from station 509 for the local orientations along the coast illustrates the effect of reorientation. As along the modeled shoreline (Figure 11b), when shadowing is neglected, local coastal orientation makes the cape flanks more stable, but does not stabilize the embayments (Figure 12b). Similar trends can be seen if different transport formulae are used, even though the Deigaard formula suggests a stable coast throughout (Figure 12c).

[56] To illustrate the shadowing effect, data from a series of WIS stations located closer to the coast, at depths typically around 20 m, represent local wave climates sheltered by the capes. Local climates show a dramatically

increased stability suggesting that shadowing becomes particularly important within the embayments where the coast would otherwise feel an unstable wave climate based only upon their orientation (Figure 12b).

[57] However, data from these local stations are affected by more than shadowing; they are also affected by wave dissipation and refraction over the shelf. The shoreface along this curving coast does not extend past depths of 20 m, and some refraction of long-period swells up to these stations occurs over nonparallel contours, an effect not included in the model. In addition, the shadowing effect within these embayments will be accentuated by shoals that extend off of the end of each of these capes, an effect that may not be accurately captured by the WIS hindcasts. These simplified analyses assuming shore-parallel contours are used to investigate large-scale trends in wave climates, and do not resolve the effect of local bathymetric features on refraction patterns (and consequently alongshore sediment transport patterns [*Palmsten et al.*, 2003]) that can be important locally (but have alongshore scales limited by those of the bathymetric features). However, what is most notable is that the wave climate trends determined by even such a simplified analysis agree closely with those seen along the simulated capes.

4.2.5. Discussion of Carolina Cape Formation

[58] Here we have hypothesized that the evenly spaced, regular shapes of the Carolina Capes may be self-organized, arising from the instability in shoreline shape and a regionally high-angle wave climate. Scientists have long speculated about the origin and maintenance of this regular series of cuspate coastal protrusions along the North Carolina and South Carolina coasts. Early speculation focused on eddies shed off of the Gulf Stream [*Abbe*, 1895; *Gulliver*, 1896], an unlikely formation scenario due to the transient nature of such along-shelf currents [*Bumpus*, 1955]. Also looking to hydrodynamic causes, *Dolan et al.* [1979] more recently suggested that trapped edge waves may induce the formation of large-scale crescentic features as part of a cascade of rhythmic coastal features [*Dolan and Ferm*, 1968], although their example requires the existing cape-associated shoals to provide the bounding features trapping the edge waves. These hydrodynamic template models do not specifically address sediment transport processes.

[59] Other hypotheses for the formation of the Carolina Capes focus on geological inheritance. *Hoyt and Henry* [1971] note the proximity of the capes to major North Carolina rivers, and suggest that the capes are reworked delta deposits (which are in the process of being "flattened" by wave attack). *Swift* [1976] also suggests that the capes exist at the locations of deltas lobes that, although they once were in the process of flattening their plan view shape, currently experience an opposite trend with alongshore sediment transport converging at the cape tips. The cause of such a dramatic shift remains unexplained. *White* [1966] discusses the importance of relict capes and cape-associated shoals in determining the location of the current capes, through both direct inheritance and the effect of the shoal complexes on drainage basin development. The correlation between rivers and the capes is not necessarily obvious, as *Riggs* [1995] show the Paleo-Cape Fear River running directly under Cape Fear, while suggesting that Cape Hatteras corresponds with an interfluve.

[60] *McNinch and Wells* [1999] have more recently collected evidence that contradicts some of these geological inheritance hypotheses. Reconnaissance and measurements show that the shoal extending offshore from Cape Lookout (Figure 10b) is an actively growing sedimentary feature along its length, and seismic data further suggests that the shoals consist of unconsolidated sediment overlying a ravinement surface contiguous with the rest of the shelf, suggesting that the cape-associated shoal accreted subsequent to late Holocene shoreface transgression. Although *Riggs* [1995] underscores the importance of underlying geology in locally "pinning" headland features, the capes do not appear to be eroding headlands.

[61] *McNinch and Wells* [1999] further note that Cape Lookout shoal is coupled to updrift (from the northeast) littoral transport, acting as a long-term sediment sink. Residual tidal currents caused by the plan view cuspate shoreline shape are likely responsible for the offshore-directed sediment transport across the shoal, although breaking-wave-induced alongshore sediment transport delivers sediment to the cape tip [*McNinch and Luettich*, 2000]. This offshore transport from residual tidal currents arises from the shape of the local cape, and does not require the preexistence of a cape-associated shoal. These potentially shoal-forming currents thus likely arise from the cuspate shape of the coastline; they do not suggest a formation mechanism for the cuspate shoreline itself.

[62] While geologic conceptual models do not seem adequate to completely explain the locations of or formation mechanism for the capes, they suggest an important point about the timescales of cape formation within the context of our self-organization hypothesis. The time it takes for Carolina Cape–scale features to develop from a straight coast in the simulations (~50,000 years) greatly exceeds that of the current sea level highstand (~6000 years [*Lambeck and Chappell*, 2001]). As the model does not explicitly include sea level changes, this suggests that several sea level highstands would be required for the capes to form from a hypothetical approximately straight coast. In this scenario, as sea level rises at the start of each interglacial period, the shoreline would likely intercept a variegated coast with existing cuspate shapes [*White*, 1966; *Moslow and Heron*, 1981] that could be affected by river downcutting and deltaic deposition during glacial lowstands. Deltas, as well as inherited capes, could act as finite-amplitude perturbations for the high-angle wave instability. Even large-scale bathymetric features, such as possible irregular shorelines drowned during rapid sea level rise, could affect wave refraction, resulting in alongshore variations in wave characteristics that would also serve as large-scale perturbations. The time span for an already undulating coast to self-organize into a regular series of capes would be significantly smaller than that required for the capes to form from a straight shoreline as depicted in the simulations [*Ashton and Murray*, 2006].

[63] Even if we consider the (unknown) shape of the coastline near the end of the Holocene rapid rise in sea level as an initial condition, that initial condition could be essentially forgotten as patterns of alongshore transport and the interactions leading to self-organization in the model remold the coast. (In the language of dynamical systems research, in some nonlinear systems many initial

states can evolve to the same attractor, and the features of the attractor can therefore be seen as more interesting than the initial conditions and the history of the trajectory [e.g., *Ott*, 1993]).

[64] The development of offshore-directed residual currents and the cape-associated shoals could cause the development of a negative feedback; once self-organized capes attain a sufficient size, residual tidal flows can develop that then act as a sediment sink that that could help "lock" a series of forelands at a certain wavelength. Preliminary model experiments suggest that the inclusion of sediment sinks at cape tips increases the aspect ratio of capes, but does not qualitatively change the shape of the coastline [*Ashton et al.*, 2000]. Future modeling work will be required to more thoroughly investigate the effects of cape process, the alteration of local wave climates caused by the shoals, and the importance of preexisting coastline undulations. However, the similarity between local wave climate trends along both simulated and natural capes is consistent with the hypothesis that the Carolina Capes have been shaped in response to the high wave angle instability.

5. Summary

[65] Studying wave climates, we have attempted to connect the theoretical instability in shoreline shape with the morphology and wave climates of natural coasts, further examining the importance the direction of approaching waves has on coastal evolution. Although their importance is obscured by refraction that makes waves break at relatively small angles, high-angle waves influence virtually all coasts. The findings presented here suggest that the influence of high-angle waves can often be obscured by scale; for example, local examination of wave climates at a beach might suggest that low-angle waves dominate. However, high-angle waves may have shaped the larger-scale embayment the beach is located in, and would therefore be responsible for the observed low-angle climate.

[66] Introducing a metric Γ, which measures the balance between diffusive and antidiffusive behavior, we have demonstrated the importance of the high wave angle instability along some natural shorelines with examples of a flying spit, sand wave fields, and a cuspate coast. One of the primary findings is that high-angle waves constitute a significant proportion of wave climates even along straight, stable coasts, for example, constituting between 25% and 49% of the contribution to shoreline evolution at the FRF.

[67] The single flying spit of Long Point protrudes into Lake Erie with an angle resulting in a climate barely dominated by low-angle waves, while at the start and tip of this spit, sand waves appear in regions where high-angle waves dominate. Along the Carolina Capes, regional and local wave climates are consistent with model predictions, suggesting that the nonlocal interactions in the model are relevant to nature, and that the Carolina Capes may be self-organized. Despite their differences in derivation and form, different alongshore sediment transport formulae show similar trends in shoreline instability.

[68] The wave climate metrics we have introduced, however, only provide general guides for predicting shoreline stability. Possible error arises from many sources, including the variation between sediment transport relationships, the quality of wave data (for example, information lost using only peak values to represent a wave climate), and the appropriateness of applying a decadal-scale wave climate to future or past evolution. However, even if Γ cannot be precisely known, it does elucidate trends in local wave climates from one location to another that can reveal much about how a coast's shape may have evolved.

Appendix A: Deepwater Transformation of the Kamphuis and Deigaard Alongshore Sediment Transport Formulae

[69] *Kamphuis* [1991] gives a formula in terms of breaking wave values:

$$Q_s = \left(2.27 m^{0.75} d_{50}^{-0.25} T^{1.5}\right) H_{b,s}^2 \cos^{0.6}\left(\phi_b - \theta\right) \sin^{0.6}\left(\phi_b - \theta\right),$$

(A1)

where Q_s is the flux of alongshore sediment (deposited volume, m^3/s), m is the beach slope, d_{50} is the median grain size (mm), T is the wave period (s), H_b is the breaking wave height (m), ϕ_b is the breaking wave crest angle, and θ is the shoreline orientation (Figure 1). This can be reduced to quantities that change during wave refraction:

$$Q_s = K_k H_{b,s}^2 \cos^{0.6}\left(\phi_b - \theta\right) \sin^{0.6}\left(\phi_b - \theta\right),$$

(A2)

where:

$$K_k = 2.27 m^{0.75} d_{50}^{-0.25} T^{1.5}.$$

(A3)

[70] Using linear wave theory, and assuming waves are fully shallow at breaking, (A2) can be recast as

$$Q_s = K_k \left(\frac{\sqrt{g\gamma}}{4\pi}\right)^{0.32} T^{0.32} H_{0,s}^{1.84} \cos^{0.92}\left(\phi_b - \theta\right) \sin^{0.6}\left(\phi_b - \theta\right),$$

(A4)

where γ is the breaking height-to-depth ratio, and assuming

$$\cos^{0.32}\left(\phi_b - \theta\right) \approx 1.$$

(A5)

[71] The fractional, decimal powers arise mostly from the empirical nature of the formula. Combining (A4) with (4),

$$\mu = \frac{K_k}{D}\left(\frac{\sqrt{g\gamma}}{4\pi}\right)^{0.32} T^{0.32} H_{0,s}^{1.84} \{0.92 \cos^{-0.08}\left(\phi_0 - \theta\right) \\ \cdot \sin^{1.6}\left(\phi_0 - \theta\right) - 0.6 \cos^{1.92}\left(\phi_0 - \theta\right) \sin^{-0.4}\left(\phi_0 - \theta\right)\},$$

(A6)

yields the Kamphuis contributions to diffusivity. Numerically derived plots of the angle dependence in (A4) and (A6) can be seen in Figures 2a and 2b, respectively.

[72] *Deigaard et al.* [1988] provide a fit to computations for the angle dependence of deepwater waves:

$$Q_s = Q_{s,\max}\left(\sin\left\{2(\phi_0 - \theta)\left[1 - 0.4\frac{(\phi_0 - \theta)}{90°} \\ \cdot \left(1 - \frac{(\phi_0 - \theta)}{90°}\right)\right]\right\}\right)^{5/2},$$

(A7)

where

$$Q_{s,\max} = \Phi H_0 \sqrt{\beta(s-1)gd^3}, \qquad (A8)$$

where β is the bed slope, s is the relative density of the sediment, g is the acceleration of gravity, d is the sediment grain diameter, and Φ is (a fit to computations of) the dimensionless alongshore sediment transport (at the maximizing angle, $(\phi_0 - \theta) = 45°$),

$$\Phi = 0.1 \left(\frac{H_0}{d}\right)^{2.3} \left(\frac{H_0}{L_0}\right)^{1/2} \exp(-6.1w^*), \qquad (A9)$$

where L_0 is the wavelength in deep water (m), and w* is the dimensionless settling velocity:

$$w^* = \frac{w}{\sqrt{gd}}, \qquad (A10)$$

where w is the settling velocity of suspended sediment (m/s). As with the CERC and the Kamphuis formulae, the sediment-specific constants do not affect the normalized wave values. A slight period dependence does arise from the wavelength dependence in (A9).

Appendix B: Discussion of Walton and Dean's "Stability Roses"

[73] Within this paper, we compile wave metrics of coastal stability while rotating through different shoreline orientations, an analysis that resembles that of "littoral drift roses" presented by *Walton and Dean* [1973; *Rosati et al.*, 2002; *Dean and Dalrymple*, 2002], where deepwater wave values are used to compute net and gross sediment transport for a range of hypothetical shoreline orientations. Using a deepwater formulation for alongshore sediment transport similar to the one independently derived by *Murray et al.* [2001], Walton and Dean separate sediment transport into left-going and right-going components. For locations of "null" points, with zero net flux, they present two different types of climates: stable and unstable. Depending on the details of the local wave climate, perturbations to a barrier island, such as a storm breach, could either continue to grow or fill in.

[74] Although the authors do not comment on the root distinction between stable and unstable climates, they provide examples of both. Looking at these examples in terms of the change in net Q_s, for the sample stable climate $\partial Q_s/\partial\theta > 0$, and for the unstable climate $\partial Q_s/\partial\theta < 0$; they are alluding to the high-angle wave instability. Their analysis, however, obscures two important aspects of the shoreline instability: first, they suggest that the magnitude of the fluxes, and not the magnitude of the flux gradients, determines shoreline stability. Also, although null (or "nodal") points excellently illustrate negative sediment budgets, "null" points are not necessary for shoreline instability. The unstable climates presented by Walton and Dean will cause instability not just at the point of zero flux, but along a larger section of the coast where $\partial Q_s/\partial\theta < 0$.

[75] This mechanism has been suggested as a possible origin of cuspate forelands [*Rosati et al.*, 2002; *Dean and*

Dalrymple, 2002], although *Dean* [2002] has recently suggested that gradients in breaking wave heights are negligible in studies of one-line coastal evolution. Despite the similarities, this "null point" instability remains a special case of the more general high wave angle instability.

References

Abbe, C. J. (1895), Remarks on the cuspate capes of the Carolina Coast, *Proc. Boston Soc. Nat. Hist.*, *26*, 489–497.

Ardhuin, F., W. C. O'Reilly, T. H. C. Herbers, and P. F. Jessen (2003), Swell transformation across the continental shelf. Part I: Attenuation and directional broadening, *J. Phys. Oceanogr.*, *33*, 1921–1939.

Ashton, A. D., and A. B. Murray (2006), High-angle wave instability and emergent shoreline shapes: 1. Modeling of sand waves, flying spits, and capes, *J. Geophys. Res.*, *111*, F04011, doi:10.1029/2005JF000422.

Ashton, A., A. B. Murray, and J. McNinch (2000), Modeling large scale coastal morphodynamics, *Eos Trans. AGU*, *81*(48), Fall Meet. Suppl., F681.

Ashton, A., A. B. Murray, and O. Arnoult (2001), Formation of coastline features by large-scale instabilities induced by high-angle waves, *Nature*, *414*, 296–300.

Bailard, J. A. (1984), A simplified model for longshore sediment transport, *Proc. Int. Coastal Eng. Conf.*, *19th*, 1454–1470.

Bumpus, D. F. (1955), The circulation over the continental shelf south of Cape Hatteras, *Eos Trans. AGU*, *36*, 601–611.

Coakley, J. P. (1992), Holocene transgression and coastal-landform evolution in northeastern Lake Erie, Canada, in *Quaternary Coasts of the United States: Marine and Lacustrine Systems*, edited by C. H. I. Fletcher and J. Wehmiller, *Spec. Publ. SEPM Soc. Sediment. Geol.*, *48*, 415–426.

Davidson-Arnott, R. G. D., and H. E. C. Reid (1994), Sedimentary processes and the evolution of the distal bayside of Long Point, Lake Erie, *Can. J. Earth Sci.*, *31*, 1461–1473.

Davidson-Arnott, R. G. D., and A. G. Van Heyningen (2003), Migration and sedimentology of longshore sandwaves, Long Point, Lake Erie, Canada, *Sedimentology*, *50*, 1123–1137.

Dean, R. G. (2002), *Beach Nourishment: Theory and Practice*, World Sci., Hackensack, N. J.

Dean, R. G., and R. A. Dalrymple (2002), *Coastal Processes With Engineering Applications*, Cambridge Univ. Press, New York.

Deigaard, R., J. Fredsoe, and I. B. Hedegaard (1988), Mathematical model for littoral drift, *J. Waterw. Port Coastal Ocean Eng.*, *112*, 351–369.

Dolan, R., and J. C. Ferm (1968), Crescentic landforms along the Atlantic Coast of the United States, *Science*, *159*, 627–629.

Dolan, R., B. Hayden, and W. Felder (1979), Shoreline periodicities and edge waves, *J. Geol.*, *87*, 175–185.

Driver, D. B., R. D. Reinhard, and J. M. Hubertz (1991), Hindcast wave information for the Great Lakes: Lake Erie, *WIS Rep. 22*, Coastal Eng. Res. Cent., U.S. Army Corps of Eng., Vicksburg, Miss.

Falqués, A., and D. Calvete (2005), Large-scale dynamics of sandy coastlines: Diffusivity and instability, *J. Geophys. Res.*, *110*, C03007, doi:10.1029/2004JC002587.

Fredsoe, J., and R. Deigaard (1992), *Mechanics of Coastal Sediment Transport*, 369 pp., World Sci., Hackensack, N. J.

Grove, R. S., C. J. Sonu, and D. H. Dykstra (1987), Fate of a massive sediment injection on a smooth shoreline at San Onofre, California, in *Coastal Sediments '87*, pp. 531–538, Am. Soc. of Civ. Eng., Reston, Va.

Gulliver, F. P. (1896), Cuspate forelands, *Geol. Soc. Am. Bull.*, *7*, 399–422.

Hoyt, J. H., and V. J. Henry (1971), Origin of capes and shoals along the southeastern coast of the United States, *Geol. Soc. Am. Bull.*, *82*, 59–66.

Hubertz, J. M. (1992), User's guide to the Wave Information Studies (WIS) Wave Model, version 2.0, *WIS Rep. 27*, 38 pp., Coastal Eng. Res. Cent., U.S. Army Corps of Eng., Vicksburg, Miss.

Inman, D. L. (1987), Accretion and erosion waves on beaches, *Shore Beach*, *55*, 61–66.

Kamphuis, J. W. (1991), Alongshore sediment transport rate, *J. Waterw. Port Coastal Ocean Eng.*, *117*, 624–640.

Komar, P. D. (1971), The mechanics of sand transport on beaches, *J. Geophys. Res.*, *76*, 713–721.

Komar, P. D. (1998), *Beach Processes and Sedimentation*, 2nd ed., 544 pp., Simon and Schuster, Upper Saddle River, N. J.

Komar, P. D., and D. L. Inman (1970), Longshore sand transport on beaches, *J. Geophys. Res.*, 75, 5914–5927.

Lambeck, K., and J. Chappell (2001), Sea level change through the last glacial cycle, *Science*, 292, 679–686.

Lippmann, T. C., and R. A. Holman (1990), The spatial and temporal variability of sand bar morphology, *J. Geophys. Res.*, 95, 11,575–11,590.

McNinch, J. E., and R. A. Luettich (2000), Physical processes around a cuspate foreland headland: Implications to the evolution and long-term maintenance of a cape-associated shoal, *Cont. Shelf Res.*, 20, 2367–2389.

McNinch, J., and J. T. Wells (1999), Sedimentary processes and depositional history of a cape-associated shoal, Cape Lookout, North Carolina, *Mar. Geol.*, 158, 233–252.

Moslow, T. F., and S. D. Heron (1981), Holocene depositional history of a microtidal cuspate foreland cape: Cape Lookout, North Carolina, *Mar. Geol.*, 41, 251–270.

Murray, A. B., A. Ashton, and O. Arnoult (2001), Large-scale morphodynamic consequences of an instability in alongshore transport, in *2nd IAHR Symposium on River, Coastal and Estuarine Morphodynamics*, pp. 355–364, Int. Assoc. of Hydraul. Res., Madrid.

Ott, E. (1993), *Chaos in Dynamical Systems*, Cambridge Univ. Press, New York.

Palmsten, M., A. Sallenger, and P. Howd (2003), Longshore currents and shoreline change: Outer Banks of North Carolina, in *Proceedings of the International Conference on Coastal Sediments 2003* [CD-ROM], World Sci., Hackensack, N. J.

Pelnard-Consideré, R. (1956), Essai de theorie de l'evolution des formes de rivage en plages de sable et de galets, in *4th Journees de l'Hydraulique, Les Energies de la Mer, III*, pp. 289–298, La Houille Blanche, Grenoble, France.

Resio, D. T. (1981), The estimation of wind-wave generation in a discrete spectral model, *J. Phys. Oceanogr.*, 2, 193–204.

Riggs, S. R. (1995), Influence of inherited geologic framework on barrier shoreface morphology and dynamics, *Mar. Geol.*, 126, 213–234.

Rosati, J. D., T. L. Walton, and K. Bodge (2002), Longshore sediment transport, in *Coastal Engineering Manual*, part II, *Coastal Sediment Processes*, edited by D. B. King, chap. III-2, U.S. Army Corps of Eng., Washington, D. C.

Ruessink, B. G., and M. C. J. L. Jeuken (2002), Dunefoot dynamics along the Dutch coast, *Earth Surf. Processes Landforms*, 27, 1043–1056.

Stewart, C. J., and R. G. D. Davidson-Arnott (1988), Morphology, formation and migration of longshore sandwaves: Long Point, Lake Erie, Canada, *Mar. Geol.*, 81, 63–77.

Swift, D. J. P. (1976), Coastal sedimentation, in *Marine Sediment Transport and Environmental Management*, edited by D. J. Stanley and D. J. P. Swift, p. 602, John Wiley, Hoboken, N. J.

Thevenot, M. M., and N. C. Kraus (1995), Longshore sand waves at Southampton Beach, New York: Observation and numerical simulation of their movement, *Mar. Geol.*, 126, 249–269.

van Enckevort, I. M. J., et al. (2004), Observations of nearshore crescentic sandbars, *J. Geophys. Res.*, 109, C06028, doi:10.1029/2003JC002214.

Walton, T. L., Jr., and R. G. Dean (1973), Application of littoral drift roses to coastal engineering problems, paper presented at First Australian Conference on Coastal Engineering, Natl. Comm. on Coastal and Ocean Eng., Inst. of Eng., Sydney, N. S. W., Australia.

Werner, B. T. (1999), Complexity in natural landform patterns, *Science*, 284, 102–104.

White, W. A. (1966), Drainage asymmetry and the Carolina Capes, *Geol. Soc. Am. Bull.*, 77, 223–240.

Wright, L. D., and A. D. Short (1984), Morphodynamic variability of surf zones and beaches: A synthesis, *Mar. Geol.*, 56, 93–118.

Zenkovich, V. P. (1959), On the genesis of cuspate spits along lagoon shores, *J. Geol.*, 67, 269–277.

Zenkovich, V. P. (1967), *Processes of Coastal Development*, Oliver and Boyd, White Plains, N. Y.

————————————

A. D. Ashton, Department of Geology and Geophysics, Woods Hole Oceanographic Institution, MS 22, Woods Hole, MA 02543, USA. (aashton@whoi.edu)

A. B. Murray, Division of Earth and Ocean Sciences, Nicholas School of the Environment and Earth Sciences, Duke University, Durham, NC 27708, USA.